

# Lumbar Spinal Stenosis CAD from Clinical MRM and MRI Based on Inter- and Intra-Context Features with a Two-Level Classifier

Jaehan Koh, Raja' S. Alomari, Vipin Chaudhary<sup>a</sup> and Gurmeet Dhillon, MD<sup>b</sup>

<sup>a</sup>Department of Computer Science and Engineering, University at Buffalo, SUNY, Buffalo, NY 14260, USA

{jkoh, ralomari, vipin}@buffalo.edu

<sup>b</sup>Proscan Imaging of Buffalo, Williamsville, NY 14221, USA  
gdhillon@proscan.com

## ABSTRACT

An imaging test has an important role in the diagnosis of lumbar abnormalities since it allows to examine the internal structure of soft tissues and bony elements without the need of an unnecessary surgery and recovery time. For the past decade, among various imaging modalities, magnetic resonance imaging (MRI) has taken the significant part of the clinical evaluation of the lumbar spine. This is mainly due to technological advancements that lead to the improvement of imaging devices in spatial resolution, contrast resolution, and multi-planar capabilities. In addition, noninvasive nature of MRI makes it easy to diagnose many common causes of low back pain such as disc herniation, spinal stenosis, and degenerative disc diseases. In this paper, we propose a method to diagnose lumbar spinal stenosis (LSS), a narrowing of the spinal canal, from magnetic resonance myelography (MRM) images. Our method segments the thecal sac in the preprocessing stage, generates the features based on inter- and intra-context information, and diagnoses lumbar disc stenosis. Experiments with 55 subjects show that our method achieves 91.3% diagnostic accuracy. In the future, we plan to test our method on more subjects.

**Keywords:** Lumbar Spinal Stenosis, CAD, MRI, MRM, Feature Generation, Classifier Design

## 1. INTRODUCTION

Low back pain is the second most common disorder encountered by clinicians after a common cold. More than a half of individuals were reported to suffer from low back pain at some time during their lives.<sup>1,2</sup> To diagnose the cause of the pain and examine the morphology of symptomatic areas, it is reported that more than 20 million MRI exams are executed annually in the United States and about a half of them are related to spine.<sup>3</sup> Despite the limitations of an imaging test, it has an important role in the diagnosis of lumbar abnormalities since it allows to depict the internal structure of soft tissues and bony elements without the need of an unnecessary surgery and recovery time. For the past decade, among various imaging modalities such as radiography, computed tomography (CT), MRI, and myelography, MRI has been adopted as a primary diagnostic tool in the clinical evaluation of the lumbar spine. This is mainly due to technology advances that lead to the improvement of imaging devices in spatial resolution, contrast resolution, multi-planar capabilities. Especially, MRIs are known to be most effective because it provides more anatomic sources of pain including nerves, muscles, and ligaments, than seen on X-rays or CT scans.<sup>4,5</sup> In addition, noninvasive nature of MRI attracts clinicians to choose it when determining many common causes of low back pain such as disc herniation, spinal stenosis, and degenerative disc diseases.

However, MRI cannot completely substitute conventional myelography since the conventional myelography is known to be the best choice for evaluating the compression effect on the thecal sac.<sup>6</sup> In addition, some orthopedic surgeons and neurosurgeons prefer myelography in some spinal disorders due to their superior overview.<sup>7</sup> Over the past decade, MRM has replaced the conventional myelography since it requires neither puncture nor contrast medium, causing no side effects.<sup>8</sup> MRM is a non-invasive method and known to be superior to conventional myelography, especially in the assessment of the spinal canal in the presence of cerebrospinal fluid block. In spite of its limited value, MRM can be used in detecting abnormalities of the spinal cord and examining the extradural compression of the thecal sac at each disc level as in Figure 1. However, it also has a limitation that it does not depict the morphology of intervertebral discs.

---

The research was supported in part by a grant from NYSTAR and NSF.

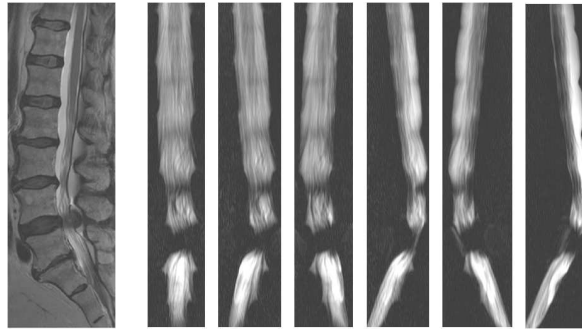


Figure 1: (a) shows a T2-weighted mid-sagittal image and (b) shows manually co-registered MRM images.

Lumbar spinal stenosis (LSS) is any type of narrowing of the lumbar spinal canal causing compression of the content of the spinal canal as in Figures 2 and 3.<sup>9,10</sup> Since a scan image in sagittal view clearly shows compressed areas along with associated disc levels, it is adopted in the initial evaluation followed by an evaluation of axial images. For example, in Figure 2, spinal canal around disc levels  $L3 - L4$ ,  $L4 - L5$ , and  $L5 - S1$  are compressed and may develop an LSS sometime in the future. In addition, in Figure 3, it is easy to diagnose if there is a compression on the spinal cord, but hard to pinpoint which disc level is associated though an LSS is detected. An LSS can be classified into two categories based on the place it occurs: *central* and *foraminal*. In the *central canal stenosis*, nerve roots in the cauda equina may be compressed. On the other hand, *foraminal stenosis* may cause compression on the nerve roots leaving the spine. Some common symptoms are low back pain, sensory disturbances in the legs, the neurogenic claudication, numbness, weakness, tingling, and radiating pain down to ankles. Pain is provoked by standing and relieved by sitting. The frequency of patients with LSS is about four times higher than that of cervical spinal stenosis and it has become the most common reason for lumbar spine surgery.<sup>11</sup> According to Boden *et al*, about 21% of asymptomatic adults at age of 60 years or older had spinal stenosis.<sup>12</sup>



Figure 2: A sagittal-view of a subject with lumbar spinal stenosis.<sup>24</sup> Figure 3: (a) shows a top-view of a normal subject while (b) shows a top-view of a subject with stenosis.<sup>23</sup>

This increasing prevalence of patients with LSS and the advancement of the imaging technology leads to a high demand for computer-aided diagnosis (CAD) for LSS so that clinicians can make accurate diagnostic decisions faster. Also, the imaging changes are reported to be more comprehensive than those from the clinical findings.<sup>13</sup> Accordingly, in this paper we propose a method to diagnose LSS from MRM and MRI images. Our methods segments thecal sac regions in the preprocessing stage, generates the features based on inter- and intra-context information, and diagnoses lumbar disc stenosis. Since the MRM does not effectively capture the structure of the thecal sac for foraminal stenosis, we give our attention only to central stenosis in this study.

## 2. RELATED WORK

Clinically, other than imaging tests, careful history and physical examinations are employed to diagnose LSS and several algorithms are reported in the literature. There are many other reported algorithms, but we only restrict our attention to the

methods mainly based on imaging studies. Jarvik and Deyo compared the performance of several algorithms in terms of specificity and sensitivity. In addition, they showed relative frequency of low back pain according to symptoms of *back pain only*, *sciatica*, or *possible stenosis*.<sup>14</sup> They also suggested an algorithm for the diagnostic evaluation of patients with low back pain using history, physical exams and imaging studies. Another comprehensive review of the diagnostic methods was done by Graaf *et al.*<sup>15</sup> They compared 15 imaging tests and 7 clinical tests in terms of the diagnostic accuracy in detecting lumbar spinal stenosis. They claimed that clinical tests showed substantial variation and there was no confirmation about the superiority of the diagnostic performance among the different tests. Wildermuth *et al* quantitatively assessed MRI and MRM in terms of the sagittal diameter of the lumbar dural sac.<sup>16</sup> Forty subjects were participated in this study and they claimed that MRI and MRM are comparable since the correlation between them is high (*i.e.*,  $r = 0.81 - 0.97$ ). They argued that there are a strong correlation between MRI and MRM but did not mention the applicability of these two modalities to CAD. Tsai *et al* introduced an automatic algorithm for the diagnosis of lumbar herniated inter-vertebral disc using a B-spine curve and features of concave and convex.<sup>17</sup> This algorithm was applied to 16 patients with CT images but did not provide neither qualitative nor quantitative analysis. Zheng *et al* introduced a new method for the quantitative evaluation of the LSS.<sup>18</sup> CT myelographic scans from 50 patients with degenerative LSS are used in the experiments. After digitizing CT scan films with a digital camera, spinal morphometry was measured using ImageTool<sup>TM</sup> software. Based on the measurements, the quantitative evaluation of LSS was conducted using computed canal cross-sectional area and dural sac canal ratio (DSCR). They concluded that mean DSCR is inversely proportional to percentile of levels decompressed. In this method, imaging processing was not done automatically and also required human intervention in obtaining measurements. Kooparirojn *et al* introduced a CAD method to diagnose LSS from sagittal MRI.<sup>19</sup> They extracted 7 features using 4 regions of interests: left/right canal heights, anteroposterior diameter, transverse diameter, upper canal width, lower canal width, lateral canal width, and ligamentum flavum thickness. Diagnosis of LSS was performed for 50 subjects using a multi-layer perceptron and they claimed the diagnostic accuracy of 92% to 97%. However, the performance analysis on the classifier was not provided. Also the selection of the axial slice was done manually by a radiologist.

Different from the previous approaches, our method works in a fully automatic fashion. A manual selection of the slice that contains the clearest snapshot of the spinal region is not necessary. Also the ROI selection, feature generation and diagnosis are carried out in a fully-automatic way.

### 3. METHOD

Our method consists of three steps: preprocessing, feature generation and diagnosis. In the preprocessing step, all MRM images are processing per patient and blobs that constitute the thecal sac are segmented. A statistical feature vector that represents the ratio of the white pixels in the window per disc level is computed in the feature generation step. Finally, a diagnosis of LSS using a two-level classifier is performed.

#### 3.1 Preprocessing

At the preprocessing step, thecal sac regions are segmented out through a set of image processing techniques as follows.

1. **ROI selection:** Since the thecal sac is located in the middle of the image, we forcibly mark the left and right regions by setting intensity values to zero. This process eliminates substantial artifacts in left- and right-hand sides of scan images. By trial and error, we found out that two sevenths of the width of the image is good enough for the left and right sides.
2. **Binarization:** The ROI is binarized based on an adaptive threshold. The threshold value for this is used based on Otsu's method.<sup>20</sup>
3. **Noise removal:** The image is smoothed by the following two-dimensional Gaussian filter  $G(x, y)$  to eliminate the effects of noise,

$$G(x, y) = \frac{1}{2\pi\sigma^2} \exp\left(-\frac{x^2 + y^2}{2\sigma^2}\right), \quad (1)$$

where  $x, y$  are image co-ordinates and  $\sigma$  is a standard deviation of the associated probability distribution.

4. **Edge detection:** Edges are extracted using Canny's edge detector.<sup>20</sup>

5. **Edge enhancement:** Edges are enhanced by a morphological dilation operator  $X \oplus S$  to form closed contours that we call *blobs*. A  $4 \times 4$  square structuring element  $S$  is used to this end.
6. **Small blobs removal:** All blobs are filled and among them small blobs are removed based on the number of pixels in each blob. Empirically, a small blob is determined to be one smaller than  $0.15 \times \max_{b_i \in B} |b_i|$  where  $b_i$  is an individual blob,  $B$  is the set of all blobs, and  $|\cdot|$  the number of pixels in a blob.

### 3.2 Feature Generation

In a clinical setting, MRI and MRM are manually co-registered by an operator, so the co-ordinates of a pixel in MRI is correspondent to the one in MRM. Considering this, the middle T2-weighted sagittal image is used to mark and label disc levels since MRM does not show intervertebral discs. That is, the labeling information manually provided in T2-weighted sagittal images are used in determining which disc level is associated with a problematic spinal canal area. Bounding boxes are generated based on one landmark point in the thecal sac region associated with each disc level as shown in Figure 4 (a). These five landmark points are employed to form bounding boxes associated disc levels in the segmentation results and used to generate a feature vector. Empirically, a height of 25 pixels are chosen. The feature vector is generated by a series of the lines that runs through the box as in Figure 4 (b). In each row in the bounding box, line segments within the box are extracted and features are generated. Specifically, per each line the fraction of foreground pixels  $f_{i,j}$  that constitutes the thecal sac is computed as

$$f_{i,j} = \frac{\text{the number of foreground pixels in line } i}{\text{the total number of pixels in line } i}, \quad (2)$$

where  $i$  represents the line index and  $j$  represent the bounding box associated with a disc level. Here,  $j$  takes on one of the following values:  $\{L1 - L2, L2 - L3, L3 - L4, L4 - L5, L5 - S1\}$ . Once  $f_{i,j}$ s are obtained, the following features are computed per bounding box: (1) minimum fraction  $\min_i f_{i,j}$ , (2) maximum fraction  $\max_i f_{i,j}$ , (3) range between the maximum fraction and the minimum fraction  $|\max_i f_{i,j} - \min_i f_{i,j}|$ , (4) mean of  $f_{i,j}$ , and (5) standard deviation of  $f_{i,j}$  from the set of lines within each box. This process is repeated for the whole set of boxes and these form our feature vector. Using this feature set, diagnosis is performed.

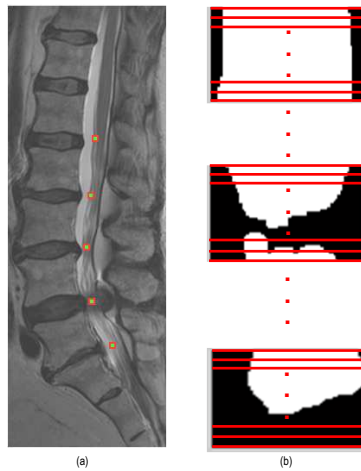


Figure 4: (a) shows a set of landmark points and (b) shows a set of lines to generate features.

### 3.3 Diagnosis

Diagnosis is performed in two levels as follows:

**Diagnosis at Level 1.** In the lower level (*i.e.*, at level 1), diagnosis is performed based on the mean range, the minimum value of the range, and standard deviation computed from the feature set of the training set, consisting of normal subjects. Since we assume that the feature vector of normal subjects follows the normal distribution if the number of subject is sufficiently large (namely, if more than 30 samples), the distribution from the training set follows the normal distribution as in Figure 7.<sup>21</sup> Based on the distribution of the range base on normal subject data,

we diagnose if the subject has a LSS associated with an intervertebral disc. Specifically, the classifier at Level 1 checks for whether there is a discontinuity in the contour of the thecal sac by evaluating if  $\min_i f_{i,j}$ ,  $\max_i f_{i,j}$  and  $|\max_i f_{i,j} - \min_i f_{i,j}|$  equal 0. Also, it checks whether each disc conforms to the statistics that are calculated by training samples as follows:

$$D_{L_1}(i, j, k) = \begin{cases} \text{LSS} & \text{if } (range_{i,j,k} < \overline{RANGE}) \text{ AND } (std_{i,j,k} > 2 \times \overline{STD}) \\ \text{normal} & \text{otherwise} \end{cases}, \quad (3)$$

where  $i$  is a patient index,  $j \in \{L1-L2, L2-L3, L3-L4, L4-L5, L5-S1\}$ , and  $k \in \{S : S \text{ is the set of images}\}$ . The  $range_{i,j,k}$  and  $std_{i,j,k}$  are statistics of the current patients while  $\overline{RANGE}$  and  $\overline{STD}$  are random variables computed from the training set, respectively. This context calculated across a set of subjects is named as *inter-context* information in our study.

**Diagnosis at Level 2.** In the higher level (*i.e.*, at Level 2), the final diagnostic decision is made by a majority voting scheme:

$$D_{L_2}(i, j) = \begin{cases} \text{LSS} & \text{if } \sum_{k=1}^{M_k} D_{L_1}(i, j, k) \geq \lfloor \frac{M_k}{2} \rfloor \\ \text{normal} & \text{otherwise} \end{cases}, \quad (4)$$

where  $i$  is the patient index,  $j$  the associated intervertebral disc,  $k$  the image slice number of MRM as discussed above, and  $M_k$  is the maximum slice number of MRM. Since  $M_k$  is 6 across all image set, the value of a floor function  $\lfloor \frac{M_k}{2} \rfloor$  equals 3. Since each MRM gives one perspective about the thecal sac, the classifier should make a decision by taking the whole MRM images into consideration. In this step, misclassification made by Level 1 is corrected. In addition, correct classification is fortified by considering classification results at Level 1 based on other slice images. Since the diagnostic decision is made only by the information of the patient himself, so we call this information as *intra-context* information. This will correct a decision mistakenly made in the lower level (*i.e.*, at level 1). An overview on our 2-level classifier is depicted in Figure 5.

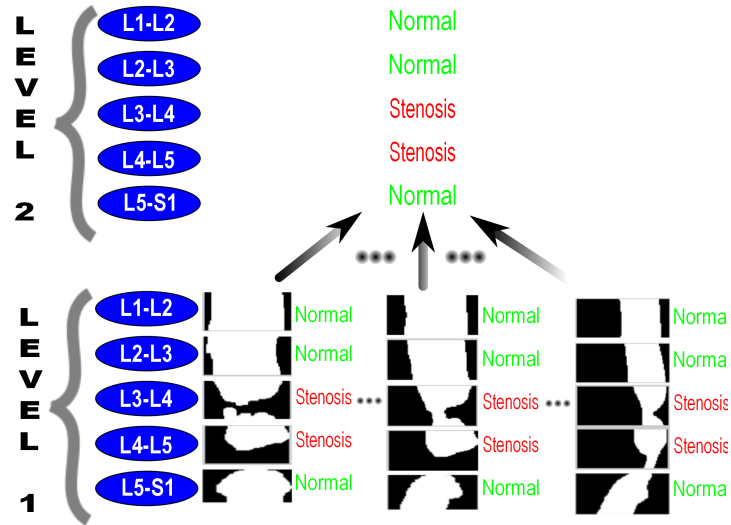


Figure 5: an overview of our 2-level classifier.

## 4. EXPERIMENT

### 4.1 Image Data and Gold Standards

The study population consist of 19 men and 36 women with a mean age of 47 years (range: 20 ~ 80 years). A total of 330 MRM images were used for diagnosis and a total of 55 T2-weighted sagittal MR images were used for creating landmark points. All images were obtained by a 3T Philips scanner that our collaborated clinic is currently using. The common parameter values for both MRI and MRM were the matrix size of  $512 \times 512$ , and flip angle of  $90^\circ$ . Other parameter values used for MRM were echo time of 1000 *ms*, repetition time of 8000 *ms*, and slice thickness of 40 *mm*. The parameters for T2-weighted sagittal were echo time of 100 *ms*, repetition time of 2622.4 *ms*, and slice thickness of 4.5 *mm*.

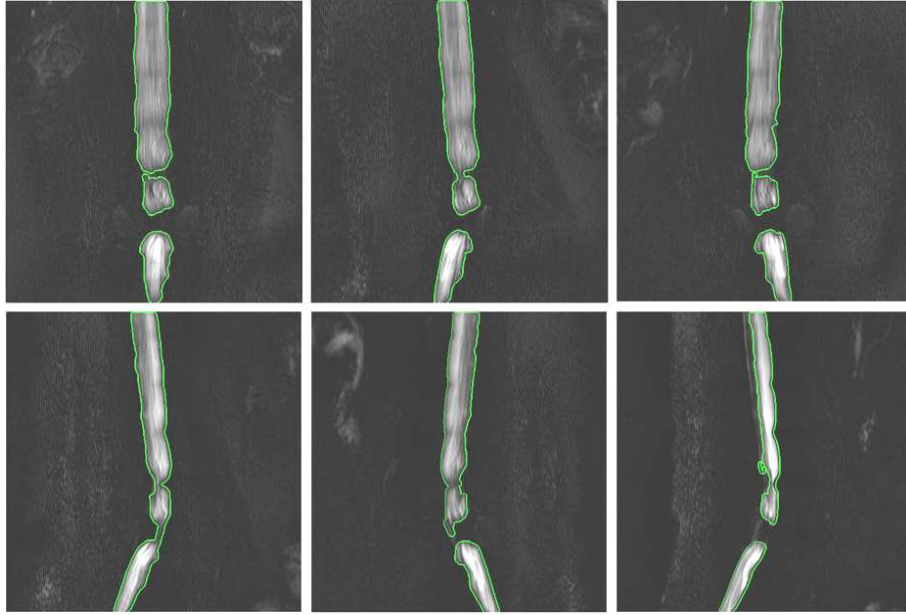


Figure 6: Segmentation results.

## 4.2 LSS Diagnosis

The classification is done through a variant of a leave-one-out method. For training of the distribution, we picked 40 subject data at random. After training, 12 subject data from the remaining were used for evaluation. This process was repeated 5 times and the diagnostic accuracy was computed. Gold standards data were constructed based on doctor's reports provided by our affiliated radiologist.

## 5. RESULTS AND DISCUSSION

Segmentation results are shown in Figure 6. As we can see, the segmented outputs accurately capture the boundary of the thecal sac despite artifacts and some level of noises.

The mean diagnostic accuracy from 5 rounds of diagnostic runs was 91.3%. As we predicted, MRM could diagnose severe central LSS very accurately. To be specific, since each MRM slice looked at the thecal sac from its own perspective, some identified the narrowing of the thecal sac while other did not. However, the big picture of the thecal sac was assessed by taking all diagnostic assessments from each MRM slice images and this two-level classifier increases the diagnostic accuracy. In addition, diagnostic mistakes made by the Level 1 classifier was corrected by our voting scheme at Level 2. However, MRM alone cannot clearly identify the causes of nerve root compression due to its intrinsic limitation that it only shows the shape of the thecal sac, not neighboring vertebrae nor intervertebral discs. An additional study with corresponding sagittal images and axial images should be followed for double-checking. However, this may be used as a primary diagnostic tool in determining which disc level has been developing LSS.

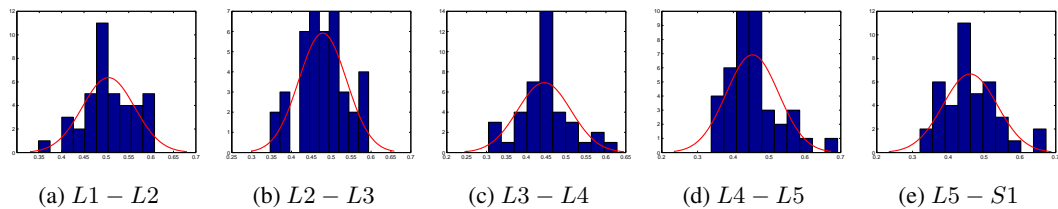


Figure 7: The distribution of a feature (*range*) per disc levels based on samples in the training set. The horizontal axis represents feature values and the vertical axis means the number of occurrences.

Disc level	L1-L2	L2-L3	L3-L4	L4-L5	L5-S1
Skewness	-0.2414	-0.0700	0.4836	1.0875	0.6693
Kurtosis	2.9813	2.8104	3.7566	4.5546	3.6456

Table 1: Skewness and kurtosis of a training set.

Disc level	L1-L2	L2-L3	L3-L4	L4-L5	L5-S1
Match rate	98%	100%	87%	60%	33%

Table 2: Match rates of diagnostic results between LSS and disc herniation.

Since our classification rules is based on the assumption that the feature set conforms to a univariate normal distribution, assessing normality of the training features is performed. To evaluate if the sample distribution follows normal distribution, two metrics are employed: *skewness* and *kurtosis*. Skewness is a measure of asymmetry of the feature set around the mean and kurtosis is a measure of the sharpness of the feature.<sup>22</sup> Skewness of a distribution is defined as

$$\mathcal{S} = \frac{E(X - E(X))^3}{\sigma^3} = \frac{\mu_3}{\sigma^3} = \frac{\mu_3}{\mu_2^{3/2}}, \quad (5)$$

where  $\mu_i$  is the  $i$ -th central moments of the feature set  $X$ ,  $\sigma$  is the standard deviation of  $X$ , and  $E(X)$  denotes the expected value of the feature set  $X$ . The skewness of the normal distribution is zero if it is perfectly symmetric. If the skewness is positive, the sample distribution is more skewed to the right of the mean to the left. On the other hand, if the skewness is negative, the sample distribution is skewed to the left.

Kurtosis of a distribution is defined as

$$\mathcal{K} = \frac{E(X - E(X))^4}{\sigma^4} = \frac{\mu_4}{\sigma^4} = \frac{\mu_4}{\mu_2^2}, \quad (6)$$

where  $\mu_i$  is the  $i$ -th central moments of the feature set  $X$ ,  $\sigma$  is the standard deviation of  $X$ , and  $E(X)$  denotes the expected value of the feature set  $X$ . The kurtosis of the normal distribution is 3. A sample distribution that gives a kurtosis greater than 3 is more outlier-dependent while a sample distribution having a kurtosis less than 3 is less outlier-dependent.

Table 1 shows the skewness and kurtosis of the feature distribution based on a training set shown in Figure 7. In disc levels  $L1 - L2$  and  $L2 - L3$ , the skewness is close to 0 and the kurtosis is about 3, implying that the feature distribution is very close to normal. In the other three disc levels  $L3 - L4$ ,  $L4 - L5$ , and  $L5 - S1$ , all the training features are distributed as normal although the distribution of  $L4 - L5$  is farthest from normal among five disc levels. One of the reasons why the sample distributions for these disc levels is less fit with a normal distribution is because LSS occurs more frequently in those three low levels and this reason makes the distribution of features more variable. If we increase the number of training samples, the sample distribution will fit with a normal distribution more closely.

The diagnosis results are evaluated through sensitivity and specificity also. Sensitivity is a measure of how likely it is for a diagnostic result to detect the presence of a disease in a subject who has it. Similarly, specificity is a measure of how likely it is for a diagnostic result to pick up the presence of a subject not having a LSS when actually one is in normal condition. The sensitivity of our classifier for the test set is 68% and the specificity for the test set is 96%. A relatively low sensitivity tells us that we need additional protocols such as a corresponding sagittal image and an axial image to diagnose LSS more accurately. In addition, we should conduct experiments on more clinical data that reflect diverse variations of LSS.

Table 2 shows the diagnostic relationship between LSS and disc herniation for the data set. As disc level gets higher the match rate gets larger. For example, on average 33% of patients with LSS in  $L5 - S1$  also suffer from disc herniation in that disc level whereas 98% of patients have both conditions in  $L1 - L2$ . This is because our LSS algorithm is only based on sagittal images. Some types of stenosis can be only detected in axial images. Furthermore, other conditions than disc herniation such as bulging discs, annulus tears, spondylolysis, spondylolisthesis, fracture, and degenerative disc diseases also result in LSS. Since disc levels  $L5 - S1$  and  $L4 - L5$  are the most frequent site having a combination of above-mentioned abnormalities, the match rate is rather low compared to other disc levels.

## 6. CONCLUSIONS AND FUTURE WORKS

Recently, among various imaging modalities MRI has taken the significant part of the clinical evaluation of the lumbar spine. This is mainly due to technological advances that lead to the improvement of imaging devices in spatial resolution, contrast resolution, and multi-planar capabilities. In addition, noninvasive nature of MRI makes it easy to diagnose many common causes of low back pain such as disc herniation, spinal stenosis, and degenerative disc diseases. In this paper, we propose a method to diagnose lumbar spinal stenosis, a narrowing of the spinal canal, from magnetic resonance myelography images. Our method segments the thecal sac in the preprocessing stage, generates the features based on inter- and intra-context information, and diagnoses lumbar disc stenosis. Experiments with 55 subjects show that our method achieves 91.3% diagnostic accuracy. In the future, we plan to test our method on more subjects.

## REFERENCES

- [1] M. N. Brant-Zawadzki, S. C. Dennis, G. F. Gade, and M. P. Weinstein, "Low Back Pain," *Radiology*, vol. 217, 2000, pp. 321-330.
- [2] J. W. Freymoyer, "Back Pain and Sciatica," *N Engl J Med*, vol. 318, 1988, pp. 291-300.
- [3] D. K. Cherry, E. Hing, D. A. Woodwell, and E. A. Rechtsteiner, "National Ambulatory Medical Care Survey: 2006 Summary," *National Health Statistics Reports*, vol. 3, 2008, pp. 1-39.
- [4] T. P. Maus, "Imaging of the spine and nerve roots," *Phys Med Rehabil Clin N Am*, vol. 13, 2002, pp. 487-544.
- [5] B. J. Richmond, and T. Ghodadra, "Imaging of spinal stenosis," *Phys Med Rehabil Clin N Am*, 2003, pp. 41-56.
- [6] J. D. Fortin, and M. T. Wheeler, "Imaging in Lumbar Spinal Stenosis," *Pain Physician*, vol. 7, 2004, pp. 133-139.
- [7] K. Hergan, T. Amann, H. Vonbank, and C. Hefel, "MR-myelography: a comparison with conventional meylography," *European Journal of Radiology*, vol. 21, 1996, pp. 196-200.
- [8] J. Ramsbacher, A. M. Schilling, K.-J. Wolf, and M. Brock, "Magnetic Resonance Myelography (MRM) as a Spinal Examination Technique," *Acta Neurochir*, vol. 139, 1997, pp. 1080-1084.
- [9] J. N. Katz and M. B. Harris, "Lumbar Spinal Stenosis," *NEJM*, vol. 13, 2002, pp. 487-544.
- [10] S. Genevay and S. J. Atlas, "Lumbar Spinal Stenosis," *Best Pract and Res Clin Rheumatol*, vol. 24, 2010, pp. 253-265.
- [11] E. Siebert, H. Prüss, R. Klingebiel, V. Failli, K. M. Einhäupl and J. M. Schwab, "Lumbar spinal stenosis: syndrome, diagnostic and treatment," *Nature*, vol. 5, 2009, pp. 392-403.
- [12] S. D. Boden, D. O. Davis, T. S. Dina, N. J. Patronas, and S. W. Wiesel, "Abnormal magnetic-resonance scans of the lumbar spine in asymptomatic subjects: A prospective investigation," *J Bone Joint Surg Am*, 1990, pp. 403-408.
- [13] M. T. Modic and J. S. Ross, "Lumbar Degenerative Disk Disease," *Radiology*, vol. 244, 2007, pp. 43-61.
- [14] J. G. Jarvik, and R. A. Deyo, "Diagnostic Evaluation of Low Back Pain with Emphasis on Imaging," *Ann Intern Med*, vol. 137, 2002, pp. 586-597.
- [15] I. Graaf, A. Prak, S. Bierma-Seinstra, S. Thomas, W. Peul, and B. Koes, "Diagnosis of Lumbar Spinal Stenosis: A Systematic Review of the Accuracy of Diagnostic Tests," *Spine*, vol. 31, 2006, pp. 1168-1176.
- [16] S. Wildermuth, M. Zanetti, S. Duewell, M. R. Schmid, B. Romanowski, A. Benini, T. Böni, and J. Hodler, "Lumbar Spine: Quantitative and Qualitative Assessment of Positional (Upright Flexion and Extension) MR Imaging and Myelography," *Radiology*, vol. 207, 1998, pp. 319-398.
- [17] M.-D. Tsai, S.-B. Jou and M.-S. Hsieh, "A new method for lumbar herniated inter-vertebral disc diagnosis based on image analysis of transverse sections," *Computerised Medical Imaging and Graphics*, vol. 26, 2002, pp. 369-380.
- [18] F. Zheng, J. C. Farmer, H. S. Sandhu, and P. F. O'Leary, "A Novel Method for the Quantitative Evaluation of Lumbar Spina Stenosis," *HSS Journal*, vol. 2, 2006, pp. 136-140.
- [19] S. Koompaiojn, K. Hua, K. A. Hua, and J. Srisomboon, "Computer-Aided Diagnosis of Lumbar Stenosis Conditions," *Proc SPIE*, vol. 7624, pp. 76241C-76241C-12, 2010.
- [20] M. Sonka, V. Hlavac, and R. Boyle, *Image Processing, Analysis, and Machine Vision*, Thomson Learning, 2008.
- [21] D. Wackerly, W. Mendenhall, and R. L. Scheaffer, *Mathematical Statistics with Applications*, Duxbury Press, 2007.
- [22] S. Theodoridis, and K. Koutroumbas, *Pattern Recognition*, Academic Press, 2009.
- [23] S. Demir-Deviren, "Spinal Stenosis: Causes, diagnosis and treatment," Spine Center, University of California San Francisco, <http://knol.google.com/k/spinal-stenosis>
- [24] L. G. Lenke, and K. Bridwell, "Lumbar Spinal Stenosis - Overview," Department of Orthopaedic Surgery at Washington University School of Medicine, <http://www.spineuniverse.com/conditions/spinal-stenosis/lumbar-spinal-stenosis-overview>